Robust Contactless Human Respiration Monitoring amid Moving Individuals Using Wi-Fi

Yanjiao Li, *Member, IEEE*, Jie Zhang, *Senior Member, IEEE*, Qing Li, Yang Li, Hien Quoc Ngo, *Fellow, IEEE*, Trung Q. Duong, *Fellow, IEEE*, and Simon L. Cotton, *Fellow, IEEE*

***Abstract*—Respiratory rate is an important vital sign that can be used to determine human physiological state. In recent years, Wi-Fi-based contactless respiration monitoring has drawn significant attention due to the prevalence of wireless local area network (WLAN) infrastructure. Most existing approaches to respiration monitoring perform well in controlled environments, without the presence of additional moving individuals in the area of interest. A few recent studies have attempted to reduce the impact of other people moving in the vicinity of the target individual. However, these approaches exhibit notable limitations, such as restricting the number of interfering individuals to one, or requiring a direct wired connection between the Wi-Fi transmitter and receiver for synchronization. To address these issues, in this study, we develop a contactless respiration monitoring system using commodity Wi-Fi devices, which we name RoSense. Through a series of empirical studies, we observe that the channel state information (CSI) for subcarriers is significantly affected by the presence of interfering individuals, but a small subset retain relatively clear signal patterns linked to the target's respiration. Leveraging these findings, RoSense employs a signal power-based subcarrier selection strategy to identify high-quality subcarriers. The selected subcarriers are then aligned to enhance signal gain and fused to complement the weaker periodic parts. Additionally, RoSense periodically detects the quality of subcarriers, selecting the most effective subcarriers to maximize the contribution of high-quality ones. Extensive experiments were performed in real-world settings with 10 volunteers to verify the feasibility and effectiveness of RoSense. Our results demonstrate that RoSense is able to achieve robust respiration monitoring by suppressing the impact of interfering individuals.**

***Index Terms*—Channel state information, interfering individuals, multi-subcarrier fusion, respiration monitoring.**

This work was supported in part by the project REASON+, a U.K. government funded project under the Future Open Networks Research Challenge (FONRC) sponsored by the Department of Science Innovation and Technology (DSIT), in part by the U.K. Engineering and Physical Sciences Research Council (EPSRC) through the EPSRC Hub on All Spectrum Connectivity under Grant EP/X040569/1 and Grant EP/Y037197/1, the UKRI Horizon Europe Guarantee for Marie Sklodowska-Curie Actions Postdoctoral Fellowships under Grant EP/Y027930/1, in part by the Fundamental Research Funds for the Central Universities under Grant FRF-TP-22-014A1, in part by the National Natural Science Foundation of China under Grant 62003038, in part by the State Administration of Foreign Experts Affairs Program under Grant H20251107, in part by the Canada Excellence Research Chair (CERC) Program CERC-2022-00109, and in part by the Natural Sciences and Engineering Research Council of Canada (NSERC) Discovery Grant Program RGPIN-2025-04941.

Yanjiao Li is with the Institute of Engineering Technology, University of Science and Technology Beijing, 100083 Beijing, China, and also with the School of Electronic and Electrical Engineering, University of Leeds, LS2 9JT Leeds, U.K. (e-mail: yanjiaoli@ustb.edu.cn).

Jie Zhang, Hien Quoc Ngo and Simon L. Cotton are with the Centre for Wireless Innovation, Queen's University Belfast, BT7 1NN Belfast, U.K. (e-mail: jie.zhang@qub.ac.uk, hien.ngo@qub.ac.uk, simon.cotton@qub.ac.uk).

Qing Li is with the School of Automation and Electrical Engineering, University of Science and Technology Beijing, 100083 Beijing, China (e-mail: liqing@ies.ustb.edu.cn).

Yang Li is with the School of Computer Science, Peking University, 100871 Beijing, China (e-mail: liyang@stu.pku.edu.cn).

Trung Q. Duong is with the Faculty of Engineering and Applied Science, Memorial University, St. John's, NL AIC 5S7, Canada, and also with the Centre for Wireless Innovation, Queen's University Belfast, BT7 1NN Belfast, U.K. (e-mail: tduong@mun.ca).

I. Introduction

HUMAN respiration is a key vital sign that can provide valuable insights into people's underlying health status [1]–[5]. Like other physiological measurements, such as pulse rate, heart rate and blood pressure, respiratory activity holds diagnostic value, particularly for chronic obstructive pulmonary diseases and obstructive sleep apnea [6]–[8]. As a result, long-term real-time human respiration monitoring is in great demand to support remote healthcare applications [9]–[12].

Conventional respiration sensing modalities typically require subjects to be equipped with dedicated on-body sensors [13]–[17]. The accuracy and robustness of wearable respiration monitoring approaches enables it to be widely adopted in short-term clinical monitoring scenarios [18]–[22]. However, such sensing modality is not well-suited for long-term home-based healthcare monitoring, especially for the elderly and those with skin sensitivities or allergies [23]–[26]. The improvement of comfort and convenience for monitored subjects promotes the deployment of computer vision-based approaches. However, these methods face significant limitations in poor-illumination and non-line-of-sight conditions, and often raise privacy concerns, further limiting their practicality in certain settings [27]–[30].

The past few years have witnessed the rapid development of wireless communication technologies and the ubiquity of Wi-Fi-enabled infrastructure. Estimating respiratory rate using commodity Wi-Fi devices in a contactless and passive manner has drawn significant attention [31]–[33]. Channel state information (CSI) obtained from orthogonal frequency-division multiplexing (OFDM) subcarriers [34]–[37] is one of the commonly used descriptors of Wi-Fi signal propagation between the transmitter and receiver. As CSI is often readily available from commodity Wi-Fi devices, this has triggered extensive research into Wi-Fi-based respiration monitoring [38]–[43]. For instance, Liu et al. [44] successfully extracted the respiration information of a subject during sleep using commodity Wi-Fi devices. Wang et al. [45] leveraged the Fresnel zones to explore the impact of human location and orientation on respiration monitoring, and pointed out

that Wi-Fi-based respiration monitoring may experience poor sensing performance at certain locations, which are referred as the "blind spots". To address this challenge, Zeng et al. [46] designed FullBreath using the complementarity between CSI amplitude and phase. This was later extended in FarSenses [47] to enlarge the respiration monitoring range to 8-9 meters by utilizing the ratio of CSI measurements from two antennas. PhaseBeat, presented in [48], utilized the CSI phase difference to detect vital signs, including respiration and heartbeat. Although considerable achievements have been made, most existing approaches struggle to maintain robust performance under ambient dynamics[1] [49], [50].

In practical settings, it is common to encounter interfering individuals within the area of interest. The signal variations caused by their activities and movements are often much stronger than those induced by a subject's respiration. Moreover, the introduction of new dynamic and static multipaths will mix with the original ones, resulting in more complicated signal propagation. Only a few recent studies have attempted to provide solutions to alleviate the impact of ambient dynamics on respiration monitoring. Specifically, ExRadio [51] was designed to monitor respiration in highly dynamic environments, but it required a direct wired connection between the Wi-Fi transmitter and receiver for synchronization. This requirement hinders its practicality and deployment in real-world scenarios. Xie et al. [52] proposed a Wi-Fi sensing system capable of monitoring respiration in the presence of a moving individual. The developed system localized both the subject and interference, and a convex optimization-based beamforming method was used to mitigate the interference. However, it is effective only in scenarios involving a single interfering individual. Therefore, how to effectively suppress the impact of multiple interfering individuals remains an open research problem.

To address the aforementioned challenges, in this study, we introduce RoSense, a real-time system designed for robust human respiration monitoring in the presence of moving individuals leveraging commodity Wi-Fi devices. Our key insight into the problem is that by leveraging the complementarity of subcarriers, we can extract and fuse those that convey valuable respiration information, thereby enhancing the respiration signal patterns. Specifically, RoSense is composed of several key modules, including a data collection module, a data preprocessing module, a multi-subcarrier fusion module, and a respiratory rate estimation module. To ensure robustness, RoSense periodically evaluates the waveforms of subcarriers and selects the most appropriate ones to maximize the contribution of those that exhibit strong periodicity. The main contributions can be summarized as follows.

1) RoSense performs effectively in Wi-Fi-based respiration monitoring under conditions with multiple interfering individuals, a scenario that severely disrupts subcarrier periodicity in most existing methods.
2) To fully utilize the information provided by subcarriers, a signal power-based subcarrier selection strategy is first employed to identify the most appropriate subcarriers. These selected subcarriers are then aligned to improve the signal gain and fused to complement their weaker periodic parts. As shall be shown in the sequel, this provides an effective way to deliver signal quality improvement, significantly enhancing the sensing ability and enlarging the sensing range, even in dynamic environments with interfering individuals.
3) We design and implement RoSense on commodity Wi-Fi devices, demonstrating its suitability for deployment in practical settings. Experimental results obtained using 10 volunteers (including 5 males and 5 females) show that RoSense outperforms state-of-the-art methods, advocating for its robustness and generalization for respiration monitoring under ambient dynamics.

[1]Ambient dynamics refer to the presence of randomly moving individuals in the area of interest.

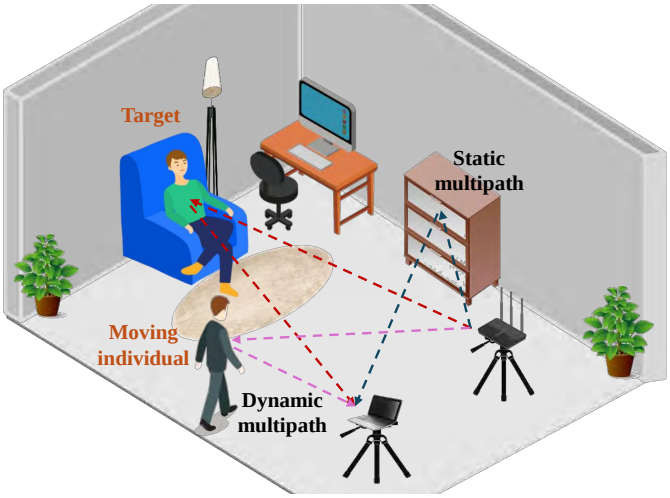

Fig. 1. Illustration of Wi-Fi-based respiration monitoring with an additional moving individual in the area of interest. The interfering individual brings new dynamic and static multipaths, and these new multipaths will mix with the original ones. Furthermore, the signal variations induced by the moving individual are often more dominant than the ones caused by the subject's respiration, thus the subtle respiratory signals are easily obscured.

The remainder of this study is organized as follows. Observations and findings are presented to facilitate the understanding of respiration monitoring under ambient dynamics in Section II. Section III details the design and implementation of RoSense, while the experimental results and analysis are reported in Section IV. Finally, discussions and conclusions are provided in Section V and Section VI, respectively.

II. Observations and Findings

In this section, we analyze the impact of ambient dynamics on respiration monitoring, and present our observations and findings to facilitate the understanding of RoSense.

A. Analysis of the Impact of Ambient Dynamics on Respiration Monitoring

When a single static subject is present in the area of interest, the signals continuously emitted from the transmitter propagate along multiple paths to the receiver and are responsible for shaping the CSI. The received signal is formed through the superposition of these different components which may include

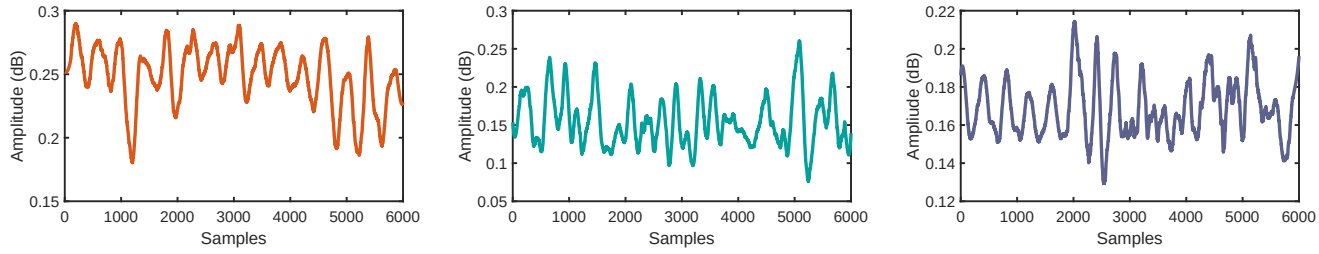

(a) (b) (c)

Fig. 2. Results of empirical studies with a moving individual in the area of interest: (a) The distance between the target and the moving individual is 6 meters; (b) The distance between the target and the moving individual is 2 meters; (c) The distance between the target and the moving individual is 1 meter.

the line-of-sight (LoS) signal component, environmental reflections, and dynamic reflection paths caused by the subject's chest movement during exhalation and inhalation. In such a scenario, improving the signal-to-noise ratio (SNR) of Wi-Fi signals can enhance sensing performance [53]–[55]. However, as shown in Fig. 1, real-world environments are often more complex, with the presence of interfering individuals such as family members, friends, caregivers, doctors, or nurses. Their activities and movements introduce new dynamic and static multipaths, which mix with the original ones. Furthermore, the signal variations caused by these activities and movements are often much stronger than those induced by the subject's respiration. As a result, the subtle respiratory signals can be easily obscured, posing a significant challenge to effective monitoring.

B. Empirical Study of Respiration Monitoring under Ambient Dynamics

To better illustrate the impact of an interfering individual on respiration monitoring, we performed an empirical study with an individual moving within the area of interest. In the experiment, the LoS length is 1.7 meters, and the target was located 5 meters away from the LoS in the perpendicular direction. The interfering individual walked randomly at distances of 6 meters, 2 meters and 1 meter from the target. We selected FarSense [47] as the baseline; it leverages the CSI ratio to improve the SNR of Wi-Fi signals. The results of the respiration signal waveforms are shown in Fig. 2. From Fig. 2, it can be observed that the signal patterns remain relatively clear when the interfering individual moves at a distance of 6 meters from the target; it means that it is still possible to ascertain the target's respiration using such signals. However, FarSense struggles to achieve satisfactory performance when the individual is within 2 meters of the target.

According to the analysis and experimental results discussed above, most existing Wi-Fi-based respiration sensing methods fail to maintain robustness under ambient dynamics. This limitation is primarily caused by the fact that such interference disrupts the statistical characteristics of Wi-Fi signals, and the subtle signal variations induced by target's respiration are easily buried by the signal variations caused by the movements of moving individuals. This makes the respiration monitoring more difficult and challenging.

C. Respiration Signal Patterns of Subcarriers under Ambient Dynamics

To provide a more intuitive demonstration of the impact of a moving individual within the area of interest on signal quality, Fig. 3 presents the amplitude waveforms of the subcarriers from one antenna on the receiver. We observe that the amplitude waveforms of most subcarriers are significantly affected by the presence of the interfering individual. It is noteworthy that a few available subcarriers exhibit relatively clear signal patterns, such as the 3rd, 5th, 6th, 7th and 8th subcarriers. Despite this clarity, these subcarriers cannot be directly used for respiration monitoring, as certain segments of their waveforms exhibit unclear respiration patterns with random fluctuations. Interestingly, we find that the weak periodicity in some segments of these subcarriers can be perfectly complemented by the corresponding good periodicity in other subcarriers. For instance, the initial portion of the 3rd subcarrier's waveform is prone to fluctuation not corresponding to respiration, while the corresponding segments of the 5th, 6th and 7th subcarriers display better periodicity. Similarly, we can hardly see the periodicity in the tail segments of the 5th and 9th subcarriers, but the corresponding segment of the 3rd subcarrier demonstrates better periodicity. It is worth emphasizing that the impact of ambient dynamics is not uniformly distributed across all subcarriers. Most subcarriers are strongly disrupted by interfering individuals, but a small subset still preserves relatively clear periodic patterns. More importantly, these subcarriers exhibit complementary characteristics: the segments with weak periodicity in one subcarrier can often be compensated by the corresponding segments with stronger periodicity in other subcarriers. These observations and findings highlight the potential of fully leveraging the inherent complementarity among available subcarriers to construct enhanced respiration signal patterns, motivating us to exploit this synergy for robust respiration monitoring.

III. Methodology

In this section, we detail the design and implementation of RoSense, which consists of the data collection module, the data preprocessing module, the multi-subcarrier fusion module, and the respiratory rate estimation module.

A. System Overview

Fig. 4 provides an overview of RoSense. Specifically, the data collection module collects raw CSI measurements using

commodity Wi-Fi devices. These collected CSI measurements are then fed into the data preprocessing module for CSI ratio construction and denoising purposes. Subsequently, the multi-subcarrier fusion module performs subcarrier selection, alignment and fusion to enhance the sensing ability and enlarge the sensing range of RoSense. The refined patterns generated by this process are then used in the respiratory rate estimation module, which employs the power spectrum density (PSD)-based estimation to accurately identify the human respiration with high robustness.

B. Data Collection

In RoSense, CSI measurements were collected using a Gigabyte mini PC equipped with an Intel 5300 network interface card (NIC) and three omnidirectional antennas. The NIC was configured to operate at a central frequency of 5.24 GHz with a bandwidth of 20 MHz. During data collection, the sample rate was set to 100 Hz. All CSI measurements were transmitted to a laptop via TCP/IP socket. Once the connection between the laptop and the receiver was successfully established, the receiver continuously sent data packets to the laptop in real-time.

C. Data Preprocessing

The CSI measurements are often contaminated by various types of noise, such as impulse noise in the CSI amplitude and random offset in the CSI phase, etc. The data preprocessing module is used to mitigate the impact of noises on sensing performance. Existing approaches often rely on simple filtering or heuristic-based methods, which lack adaptability to varying noise conditions and may fail in complex real-world scenarios. To address these limitations, we employ a systematic preprocessing strategy that includes outlier removal, trend elimination, and signal smoothing. This ensures that only meaningful respiration information is retained.

RoSense utilizes the CSI ratio as the base signal, which can be calculated as [56]

$$\begin{aligned}\frac{H_1(f,t)}{H_2(f,t)} &= \frac{e^{-j\mu_{offset}}(H_{s,1}+A_1e^{-j2\pi\frac{d_1(t)}{\lambda}})}{e^{-j\mu_{offset}}(H_{s,2}+A_2e^{-j2\pi\frac{d_2(t)}{\lambda}})} \\ &= \frac{A_1e^{-j2\pi\frac{d_1(t)}{\lambda}}+H_{s,1}}{A_2e^{-j2\pi\frac{d_1(t)+\Delta d}{\lambda}}+H_{s,2}} \\ &= \frac{A_1e^{-j2\pi\frac{d_1(t)}{\lambda}}+H_{s,1}}{A_2e^{-j2\pi\frac{\Delta d}{\lambda}}e^{-j2\pi\frac{d_1(t)}{\lambda}}+H_{s,2}}\end{aligned} \tag{1}$$

where $H_1(f,t)$ and $H_2(f,t)$ are the CSIs of the first antenna and second antenna, $H_{s,1}$ and $H_{s,2}$ are the corresponding static phasor components, A_1 and A_2 represent the complex attenuation, $d_1(t)$ and $d_2(t)$ represent the propagation lengths, and $e^{-j\mu_{offset}}$ denotes the time-varying random phase offset.

As mentioned above, the collected CSI signals are often contaminated by environmental noise and hardware noise, causing some CSI samples to deviate from the majority of CSI samples within the same subcarrier. To remove these anomalies, a Hampel filter was employed to detect and eliminate outliers. The Hampel filter is a median absolute deviation (MAD)-based filter that handles outliers and noise [57]. It does not require the assumption that the collected data follows a Gaussian distribution. Additionally, the median, as an unbiased estimator, is highly resistant to interference from extreme values and outliers. This makes the Hampel filter well-suited for CSI data filtering, as it effectively identifies and suppresses sudden deviations while preserving true respiratory fluctuations.

Letting $\{X\} = \{x_1, x_2, \ldots, x_q\}$ with q elements be the CSI ratio dataset, the MAD is

$$MAD = median\{|x_i - x_{median}|\} \tag{2}$$

where x_{median} denotes the median value of $\{X\}$.

The MAD scale estimate is represented as

$$T_{MAD} = \frac{\kappa|x_i - x_{median}|}{MAD} \tag{3}$$

where $\kappa = \frac{1}{\sqrt{2}erfc^{-1}(1/2)} \approx 1.4826$. It enables T_{MAD} to be an unbiased estimate of the standard deviation for Gaussian data. Based on our observations, when T_{MAD} is larger than 1, we consider the corresponding CSI measurement to be an outlier.

After removing outliers, the Savitzky-Golay (S-G) filter was applied to reduce environmental noise and further smooth the CSI ratio, while preserving the envelope of the original waveform. The S-G filter has two adjustable degrees of freedom, including the data window size and the polynomial order. In this study, we configured the S-G filter with a polynomial order of 3 and a window size of 201 to achieve optimal smoothing performance.

To address the random offset present in the CSI phase, median filtering was employed to detrend the data, leaving the signal fluctuations. It utilizes the median of each sample within a sliding window to replace the target sample. During the filtering process, the CSI measurements were normalized to have a mean of 0 and a standard deviation of 1.

The detailed steps of the data filtering are as follows.

Step 1: Extract the raw CSI complex matrices from data packets, and then compute the CSI ratio by dividing the received CSI measurements from any two of the three antennas on the receiver;

Step 2: Apply the Hampel filter to eliminate the impact of noise on the collected data;

Step 3: Use the S-G filter to reduce the environmental noise and smooth the data;

Step 4: Employ the median filter to eliminate the signal trend items.

These preprocessing steps collectively refine the extracted respiratory patterns, ensuring greater clarity and reliability while establishing a solid foundation for accurate respiratory rate estimation.

D. PSD-based Multi-Subcarrier Fusion

After data preprocessing, the trend components and the majority of noise in the CSI data are eliminated. The multi-subcarrier fusion module was then employed mainly to maximize the contribution of high-quality subcarriers through

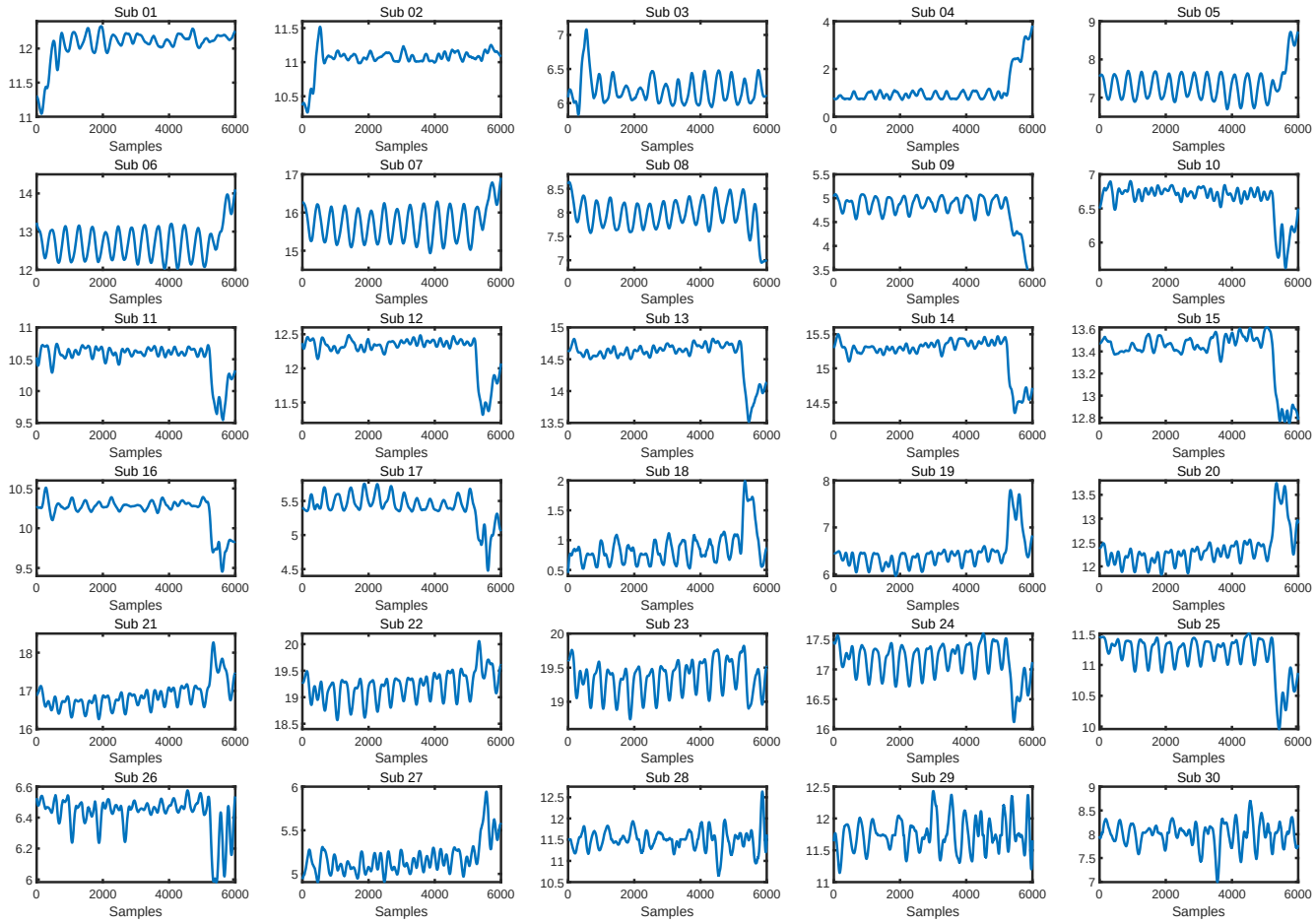

Fig. 3. Signal waveforms of subcarriers in the presence of a moving individual in the area of interest. While many subcarriers are disrupted by the interfering individual, a few available subcarriers exhibit relatively clear signal patterns.

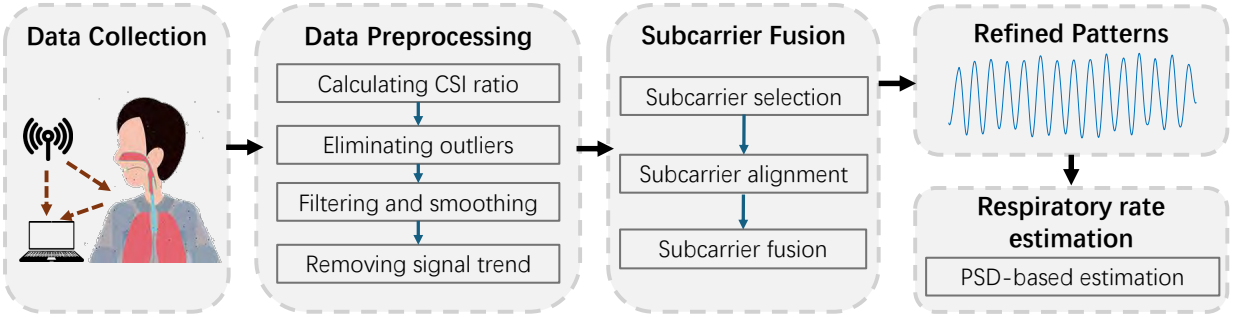

Fig. 4. System overview of RoSense. RoSense consists of several functional modules, including the data collection module, the data preprocessing module, the mulit-subcarrier combination module, and the respiratory rate estimation module.

combining all the available subcarriers into a unified representation.

1) Subcarrier Selection: Given the number of antennas on the transmitter N_{Tx} and receiver N_{Rx}, we obtain $N_{Tx} \times N_{Rx} \times 30$ CSI readings at each time stamp, i.e., a total of 90 CSI readings. Since not all subcarriers exhibit strong and stable respiratory signatures, as illustrated in Fig. 3, it is crucial to implement an effective selection mechanism to identify the most reliable ones for respiration sensing.

The chest movement caused by human respiration is periodic in the time domain. When these periodic fluctuations align with the frequency of human respiration, the corresponding CSI signals are considered suitable for respiration sensing. To identify subcarriers that effectively represent human respiration, the PSD is utilized to analyze the CSI signals in the frequency domain. The appropriate subcarriers were selected based on the peak values of PSD. It should be noted that a desirable waveform for respiration is sinusoidal/cosinusoidal in nature, which manifests a sharp peak within the normal respiratory frequency range in its PSD. However, empirical analysis reveals that the subcarrier with the highest PSD value does not necessarily correspond to the strongest periodic

respiratory signal. This is because the total power of a signal includes not only the respiration-induced component but also contributions from environmental interference and random fluctuations. As a result, relying solely on the highest PSD magnitude may lead to the selection of subcarriers that do not accurately capture respiration-related periodic patterns. Therefore, multiple subcarriers with appropriate PSD characteristics were selected to provide complementary information, ensuring more robust and accurate respiration sensing.

We calculated the peak value of the PSD of each subcarrier PSD_n ($n = 1, 2, \ldots, 90$), and checked its maximum value:

$$PSD_{max} = max\{PSD_n\} \tag{4}$$

After that, considering the fluctuations of the performance for different sensing distances, we set a threshold θ to select the most appropriate subcarriers.

$$\theta = \begin{cases} PSD_{max} - \psi_1, & PSD_{max} > 0.5 \\ PSD_{max} - \psi_2, & PSD_{max} \leq 0.5 \end{cases} \tag{5}$$

If the subcarrier satisfies the following criterion, then it becomes a candidate:

$$PSD_n - \theta \geq 0 \tag{6}$$

The process of subcarrier selection is depicted in Algorithm 1.

Algorithm 1 Subcarrier Selection

Input: Preprocessed subcarriers, thresholds ψ_1 and ψ_2, window length $\tilde{T}$.

Output: Selected subcarriers

1: Calculate the peak value of the PSD for each subcarrier PSD_n.
2: Identify the maximum value of peak value PSD_{max}.
3: Detect and retain subcarriers satisfying the criterion defined in Eq. (6).
4: Output the selected subcarriers.

Due to the spatial diversity of multipath propagation, subcarriers are impacted differently by environmental dynamics. Consequently, interference is typically non-uniform and does not impact all subcarriers coherently. Moreover, since each multipath component contributes uniquely to different subcarriers, motion-induced perturbations cause the interference distribution to evolve dynamically. To address this, RoSense periodically evaluates subcarrier quality and isolates respiration-specific frequencies, suppressing non-periodic and off-band disturbances. Every $\tilde{T}$ seconds, the system analyzes waveforms of available subcarriers and selects those meeting the required criteria, ensuring that only high-quality subcarriers are used for respiration sensing. This adaptive mechanism allows RoSense to maintain robustness despite signal quality in real-world environments. Moreover, in this study, to ensure an optimal trade-off between adaptability and stability, we empirically set ψ_1 to 0.15 and ψ_2 to 0.1, respectively. These parameters were determined through extensive experiments under diverse settings, such as different indoor environments, LoS lengths, and interfering individuals. As long as the intrinsic characteristics of human respiration (0.1-0.5 Hz) and the frequency-selective fading behavior of commodity Wi-Fi channels remain unchanged, the same parameters can be directly used without re-tuning in typical indoor scenarios. Additionally, setting $\tilde{T}$ to 60 aligns with typical respiratory cycle durations, allowing for a stable responsive estimation process.

Compared to using the breathing-to-noise ratio (BNR) as a criterion for subcarrier selection, the signal power-based subcarrier selection strategy directly evaluates the spectral energy around the respiratory frequencies. The BNR-based method relies on a prior estimation of the respiratory signal, which becomes unstable under dynamic interference. Additionally, the PSD-based criterion helps preserve subcarriers with strong respiration components, enabling the subsequent subcarrier alignment and fusion to exploit their complementarity more effectively. Moreover, the PSD peak can be easily recomputed and updated periodically to maintain real-time performance.

2) Subcarrier Alignment: We observed that there is a fixed difference (typically between 0 degrees and 180 degrees) between subcarriers, as shown in Fig. 5 (a). Prior work has demonstrated that multipath propagation introduces phase rotation across subcarriers, leading to phase shifts between them [53]. This work further establishes that subcarrier-level phase compensation restores this coherence by correcting these deterministic phase shifts. After alignment, the respiratory component becomes consistent across subcarriers and can be reinforced through superposition, while interference is suppressed. This principle aligns with the phenomena observed in our experiments, providing strong theoretical support. Therefore, it is essential to remove the differences by aligning these subcarriers before combining them. To address this issue, one subcarrier was selected as the reference, and the remaining subcarriers were aligned towards it based on their distance similarity. The subcarrier alignment process involves three key procedures:

Step 1: Select the subcarrier with the maximum peak value in the PSD as the reference subcarrier.

Step 2: Calculate the Euclidean distance between the reference subcarrier and the selected appropriate subcarriers.

Step 3: Define a pre-defined distance threshold, and invert the subcarriers whose distance from the reference exceeds the threshold.

The selection of an appropriate distance threshold is crucial for ensuring effective subcarrier alignment while minimizing unnecessary signal inversion. A statistical analysis of subcarrier phase differences across multiple testing scenarios was performed. Specifically, we observed that when the Euclidean distance between subcarriers exceeded 100, the phase deviations were substantial enough to degrade the combined signal quality. Conversely, a lower threshold risked inverting subcarriers that were already well-aligned, leading to unnecessary signal distortion. Therefore, we set the distance threshold to 100 to provide a balance between preserving meaningful phase relationships and mitigating destructive interference. Additionally, we observed that the characteristics of respiration-related CSI components are relatively stable across scenarios. As a result, the distance threshold is not highly sensitive to

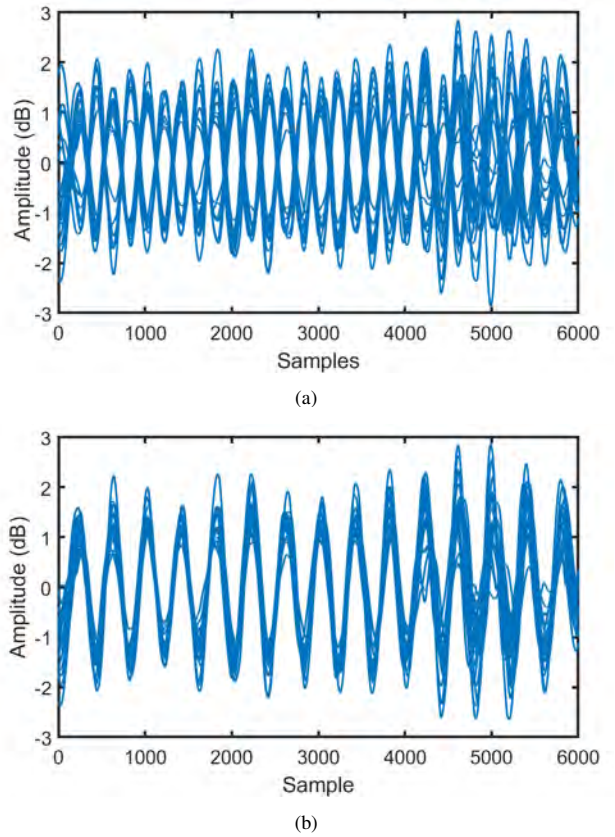

Fig. 5. Demonstration of selected subcarriers before and after the alignment: (a) There is a fixed difference between subcarriers and; (b) All the subcarriers are aligned to the reference subcarrier.

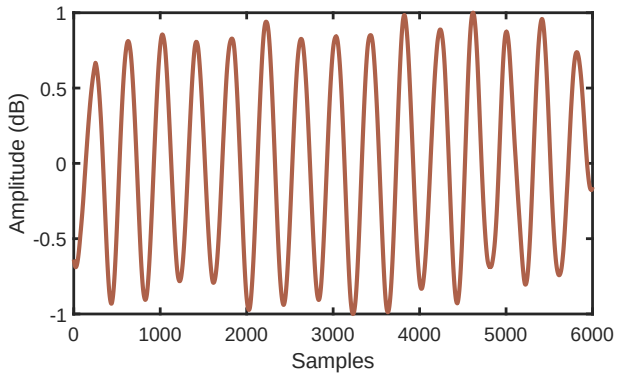

Fig. 6. Respiration signal pattern after multi-subcarrier fusion.

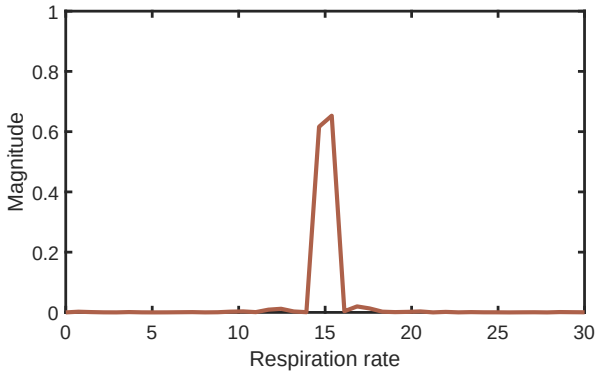

Fig. 7. Illustration of estimated respiratory rate based on PSD.

environmental changes and does not require frequent tuning. Fig. 5 (b) shows the result of the subcarrier alignment. With the above alignment, we realize the waveform synchronization for all the selected subcarriers to strengthen the signal gain.

3) Multi-Subcarrier Fusion: To further enhance the sensing performance, all the aligned subcarriers were fused to complement their weaker periodic parts. We employed a direct superposition on the aligned subcarriers. In RoSense, we found that the equal-weight superposition is sufficient because low-quality subcarriers have already been removed during the PSD-based selection, leaving only subcarriers with relatively clear and complementary periodic patterns. Additionally, weighted fusion requires additional weight estimation, which increases computational complexity and may degrade the sensing performance under dynamic interference. In our observations, direct superposition achieves a good balance between robustness, computational efficiency, and real-time performance. The fusion result is illustrated in Fig. 6. From this figure, we can see that the fused waveform exhibits significantly clearer and more distinct periodic respiration patterns. This improvement highlights the effectiveness of the multi-subcarrier fusion in amplifying the periodic components of the respiration signal, while mitigating the noise and interference. The much clearer waveform is a direct indication of the enhanced signal quality, which contributes to more accurate respiratory rate estimation.

E. Respiratory Rate Estimation

Using the fused subcarriers, the respiratory rate was estimated through PSD analysis. By performing PSD analysis on the fused signal, the time-domain data can be transformed into its frequency-domain representation. If the amplitude reaches its maximum within the range of the normal human respiration rate, i.e., 0.1 - 0.5 Hz, RoSense identifies the corresponding frequency component to calculate the respiratory rate. As shown in Fig. 7, the peak value of the signal corresponds to the estimated respiratory rate. The sharp and well-defined peak in the PSD of the fused subcarriers benefits from the enhanced signal quality, allowing for a more accurate and robust estimation of the respiratory rate.

IV. Case Study

In this section, we verify RoSense by conducting extensive experiments in various practical scenarios. Specifically, we first evaluate the performance of RoSense in the presence of one single moving individual. We then explore the impacts of (i) the LoS path length; (ii) the number of interfering individuals; (iii) the impact of an individual crossing the area between the target and the LoS path; and (iv) the sensing range of RoSense in the absence of any moving individuals. Finally, we compare RoSense with selected dynamic-interference-aware baseline methods designed to mitigate motion-induced disturbances.

TABLE I
DESCRIPTIONS OF SCENARIOS WITH/WITHOUT SINGLE/MULTIPLE INTERFERING WALKING INDIVIDUALS IN THE AREA OF INTEREST

Scenarios	Testbeds	LoS Lengths	Scenario Descriptions
S1	Laboratory	1.7 m	One interfering individual walking around the target, maintaining a distance of 2 m
S2	Laboratory	1.7 m	One interfering individual walking around the target, maintaining a distance of 1 m
S3	Corridor	1.7 m	One interfering individual walking around the target, maintaining a distance of 2 m
S4	Corridor	1.7 m	One interfering individual walking around the target, maintaining a distance of 1 m
S5	Laboratory	1.3 m	One interfering individual walking around the target, maintaining a distance of 1 m
S6	Laboratory	1.9 m	One interfering individual walking around the target, maintaining a distance of 1 m
S7	Laboratory	2.1 m	One interfering individual walking around the target, maintaining a distance of 1 m
S8	Laboratory	2.3 m	One interfering individual walking around the target, maintaining a distance of 1 m
S9	Corridor	1.3 m	One interfering individual walking around the target, maintaining a distance of 1 m
S10	Corridor	1.9 m	One interfering individual walking around the target, maintaining a distance of 1 m
S11	Laboratory	1.7 m	Two interfering individual walking around the target, maintaining a distance of 2 m
S12	Laboratory	1.7 m	Three interfering individual walking around the target, maintaining a distance of 2 m
S13	Corridor	1.7 m	Two interfering individual walking around the target, maintaining a distance of 1 m
S14	Corridor	1.7 m	Three interfering individual walking around the target, maintaining a distance of 1 m
S15	Laboratory	1.7 m	One interfering individual crossing the area between the target and the LoS path
S16	Laboratory	1.7 m	No interfering individual in the area of interest, the target-LoS distance is 10 m
S17	Corridor	1.7 m	No interfering individual in the area of interest, the target-LoS distance is 25 m
S18	Laboratory	1.5 m	One interfering individual walking around the target, maintaining a distance of 2 m
S19	Laboratory	1.5 m	Two interfering individuals walking around the target, maintaining a distance of 2 m
S20	Corridor	1.5 m	One interfering individual walking around the target, maintaining a distance of 1 m
S21	Corridor	1.5 m	Two interfering individuals walking around the target, maintaining a distance of 1 m

A. Experimental Settings

The experimental environments considered in this study included two indoor environments: a laboratory and a corridor, as shown in Fig. 8. The floor space occupied by the laboratory is 10 m $\times$ 12 m, and the width and length of the corridor are 2.5 m and 30 m. RoSense was implemented in these environments using a pair of Wi-Fi transceivers. We recruited 10 volunteers (5 males and 5 females) to participate in the experiments. To quantitatively assess the respiration monitoring performance, the mean absolute error (MAE) was considered as the evaluation criterion. MAE is defined as the mean of the absolute differences between the estimated respiratory rate and the ground truth over the entire measurement session. In the experiments, we considered various scenarios, as outlined in Table I, to investigate the effectiveness of RoSense from multiple perspectives. More scenario specifications appear in their dedicated subsections.

B. Baseline Methods

We compared RoSense with several commonly utilized respiration monitoring approaches using Wi-Fi. HRD [45], FarSense [47] and CSI ratio [58] were selected as the representative baseline methods designed for static scenarios. For dynamic-interference-aware baseline methods, we selected ExRadio [51] and RespiRadio [59].

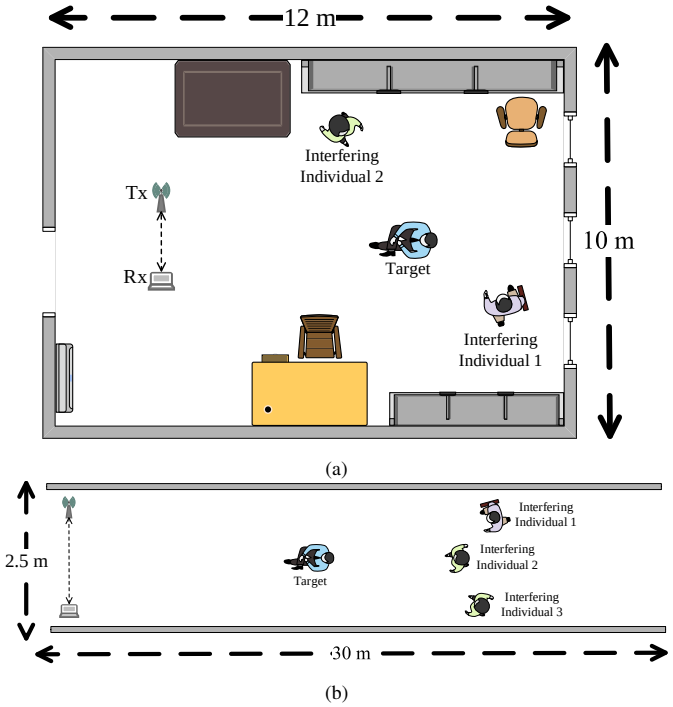

Fig. 8. Illustration of floorplan of experimental environments: (a) Laboratory, with two interfering individuals walking around the target and; (b) Corridor, with three interfering individuals walking around the target.

- **HRD.** The base signal of HRD is the CSI amplitude. HRD first employs a Hampel filter and a moving average filter to mitigate the impact of noises and outliers. Next, HRD identifies subcarriers with higher CSI amplitude variance using a threshold-based selection approach. Finally, the respiratory rate is estimated through a peak detection approach.
- **FarSense.** The base signal of FarSense is the CSI ratio. FarSense first calculates the autocorrelation of the respiration pattern for each subcarrier, and then combines the autocorrelation results across multiple subcarriers to estimate the respiratory rate.
- **CSI ratio.** This method selects subcarriers with higher CSI ratio variance, and then estimates the respiratory rate using a peak detection approach.
- **ExRadio.** The base signal of ExRadio is CSI ratio. This method introduces a wire direct connection channel between transmitter and receiver to eliminate the hardware-related noises.
- **RespiRadio.** This method synthesizes a wider-bandwidth Wi-Fi radio using commodity devices to enable highly accurate respiratory rate monitoring in dynamic environments.

C. Performance Comparison in the Presence of a Moving Individual

We conducted experiments in the two indoor environments with one interfering individual present, covering scenarios S1, S2, S3 and S4. The schematic of these scenarios is depicted in Fig. 9. The LoS path length distance was set at 1.7 meters, with the target located 5 meters away from the LoS path. An individual was asked to walk randomly within the area of interest, maintaining distances of 2 meters or 1 meter from the target.

Fig. 10 and Fig. 11 show the respiration signal patterns of RoSense compared to the three baseline methods designed for static scenarios at different distances between the target and the moving individual in both laboratory and corridor settings. According to these figures, we can see that RoSense obtains clearer signal patterns than the baseline methods in the presence of the interfering individual. The signal waveforms captured by RoSense are sinusoidal/cosinusoidal-like with much clearer periodic patterns, while the signal waveforms obtained by HRD, FarSense and CSI ratio exhibit weaker periodicity and more irregular patterns.

Fig. 12 presents the MAE of all the methods with different distances between the target and the moving individual. From Fig. 12, we can see that RoSense is superior to the baseline methods, and FarSense performs better than HRD and CSI ratio. Additionally, unlike the baseline methods, RoSense is not sensitive to the distances between the target and the moving individual. This demonstrates that RoSense is more robust and efficient in the scenarios involving a moving individual within the area of interest.

Taken together, the performance improvement achieved by RoSense can be attributed to its design. Unlike baseline methods, RoSense dynamically identifies subcarriers based on signal power variation and periodicity recognition. More precisely, RoSense performs subcarrier alignment to ensure that the selected subcarriers exhibit consistent patterns before multi-subcarrier fusion, which enhances the extraction of weak respiration-induced periodic components. In contrast, baseline methods lack such temporal alignment, resulting in unstable respiration signal extraction. These mechanisms enable RoSense to achieve stable performance even in the presence of the moving individual within the area of interest.

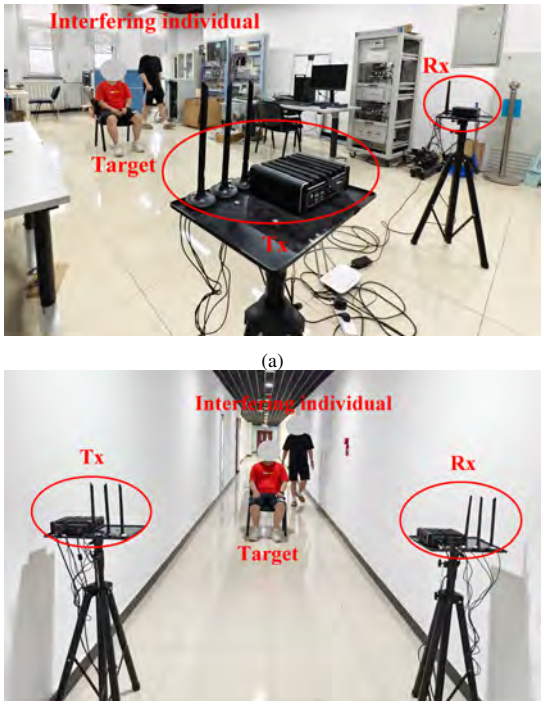

Fig. 9. Demonstration of experiments with an interfering individual in the area of interest: (a) Laboratory and; (b) Corridor.

D. Impact of Different LoS Lengths

We also explored the impact of different LoS lengths on RoSense in the presence of a moving individual, as represented by scenarios S5, S6, S7, S8, S9 and S10. Specifically, in the laboratory, the LoS path length distances were set as 1.3 meters, 1.9 meters, 2.1 meters and 2.3 meters, respectively. In the corridor, we only considered two scenarios where the LoS was 1.3 meters and 1.9 meters due to the space constraints. Fig. 13 depicts the MAE of RoSense and the baseline methods designed for static scenarios across different LoS lengths. According to Fig. 13, we find that RoSense consistently achieves the lowest MAE, and maintains stable performance across varying LoS lengths. This robustness eliminates the need for precise LoS adjustments during deployment. Consequently, users can deploy RoSense more quickly and with greater flexibility, reducing setup complexity and making it more efficient and user-friendly.

E. Impact of Number of Moving Individuals

To further verify the robustness of RoSense, we explored the impact of number of moving individuals within the area of

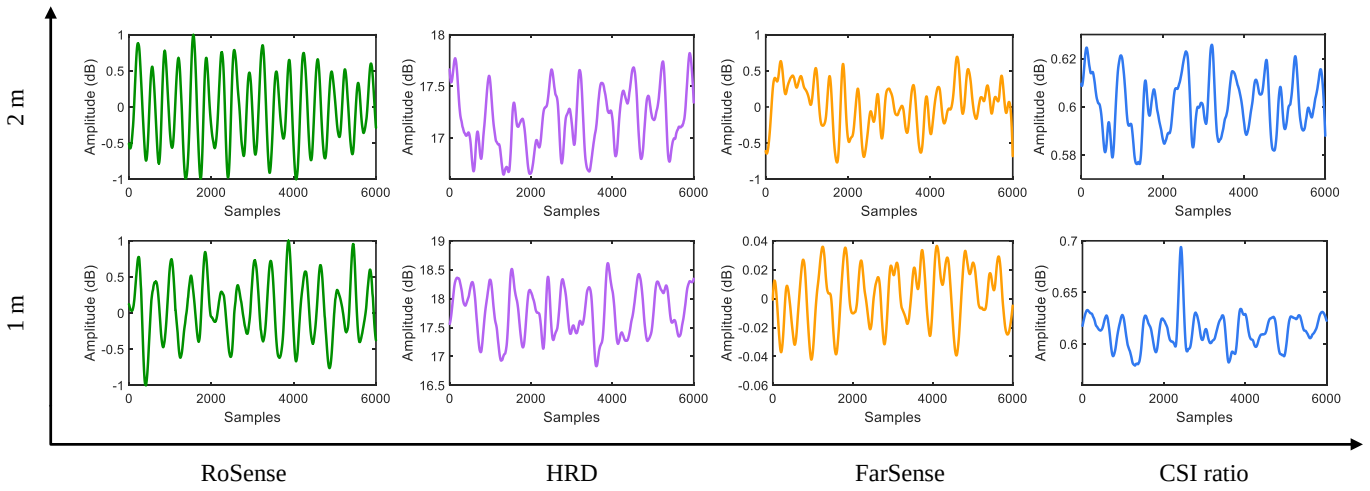

Fig. 10. Respiration signal patterns of different methods at varying distances between the target and moving individual in the laboratory (S1 and S2).

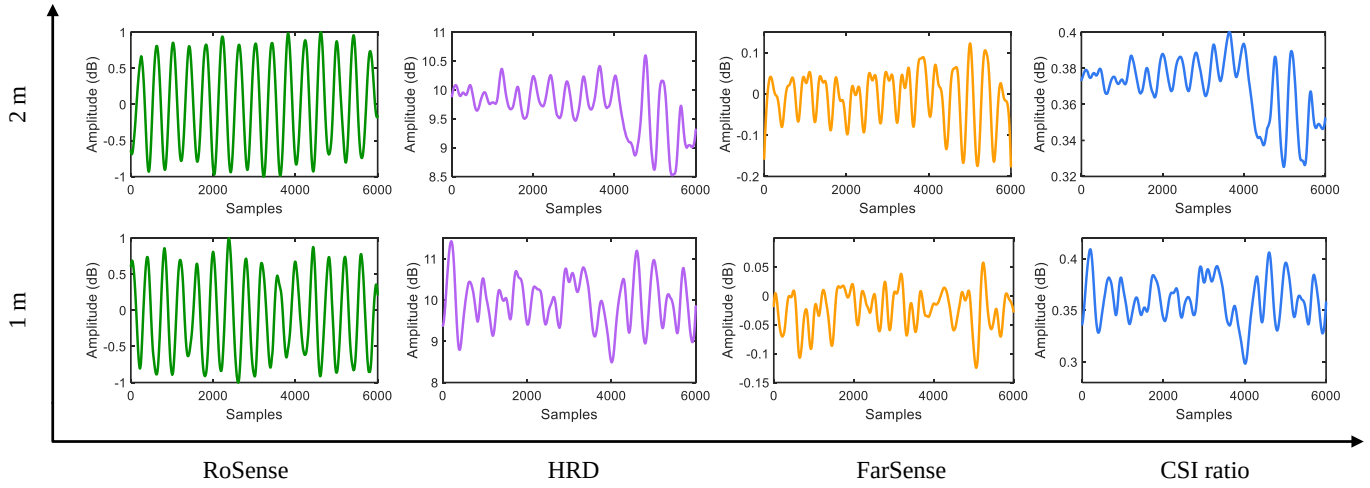

Fig. 11. Respiration signal patterns of different methods at varying distances between the target and moving individual in the corridor (S3 and S4).

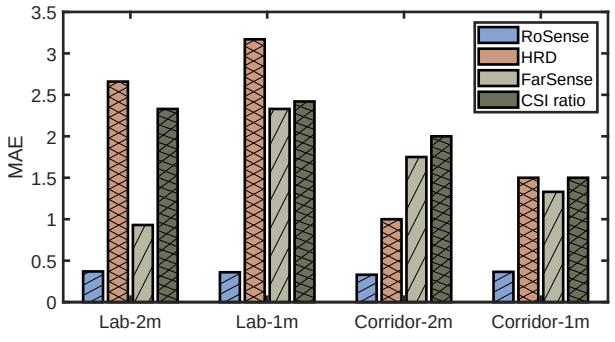

Fig. 12. MAE of RoSense and baseline methods at different distances between the target and the moving individual (S1–S4).

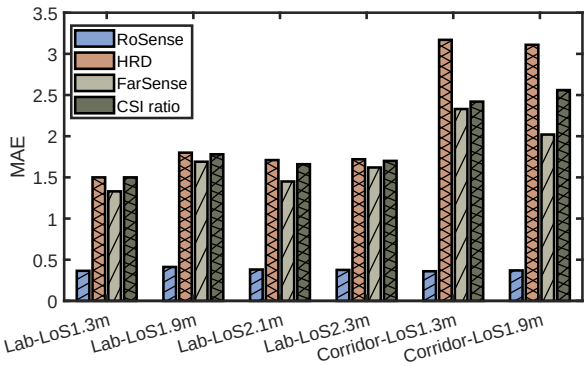

Fig. 13. MAE of RoSense and baseline methods at different LoS lengths (S5–S10).

interest. Scenarios S11, S12, S13 and S14 were constructed to evaluate RoSense under increased interference, involving two and three individuals walking randomly in the laboratory and corridor at distances of 2 meters and 1 meter from the target, as shown in Fig. 14. Table II and Table III provide the detailed MAE of RoSense and the baseline methods designed for static scenarios under these conditions. It is obvious that RoSense achieves the best performance among these methods. In the two moving individuals scenario, RoSense reduces the MAE

(a)

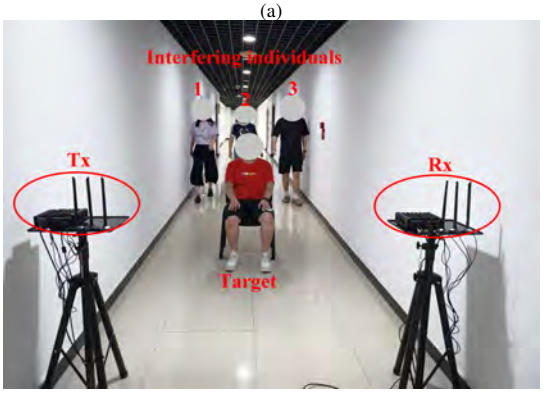

(b)

Fig. 14. Illustration of multiple interfering individuals in the area of interest: (a) Two moving individuals in the laboratory and; (b) Three moving individuals in the corridor.

TABLE II
MAE OF ROSENSE AND BASELINE METHODS DESIGNED FOR STATIC SCENARIOS IN PRESENCE OF DIFFERENT NUMBER OF MOVING INDIVIDUALS IN LABORATORY

Scenarios	RoSenses	HRD	FarSense	CSI ratio
S11	0.66	1.21	2.09	1.15
S12	0.68	2.29	1.59	1.86

by up to 68% and 75% in the laboratory and the corridor. For the scenario with three moving individuals, RoSense reduces the MAE by up to 70% and 76% in the laboratory and the corridor. These findings confirm the robustness of RoSense in challenging environments with multiple moving individuals.

F. Impact of an Individual Crossing between Target and LoS

In the scenario S15, we verified the robustness of RoSense when an individual crosses the area between the target and

TABLE III
MAE OF ROSENSE AND BASELINE METHODS DESIGNED FOR STATIC SCENARIOS IN PRESENCE OF DIFFERENT NUMBER OF MOVING INDIVIDUALS IN CORRIDOR

Scenarios	RoSenses	HRD	FarSense	CSI ratio
S13	0.72	2.97	2.76	2.35
S14	0.81	3.41	2.65	2.87

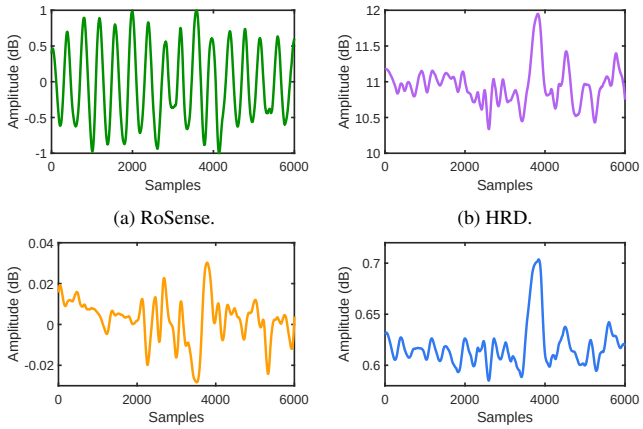

Fig. 15. Respiration signal patterns under an individual crossing the area between target and LoS, i.e., S15.

the LoS. This scenario is particularly challenging, as direct signal reflections are easily obstructed by a crossing individual. Fig. 15 depicts the respiration signal patterns of RoSense and the baseline methods designed for static scenarios. According to Fig. 15, the signal pattern obtained using RoSense exhibits good periodicity even in this scenario, whereas the baseline methods are significantly disrupted by the crossing individual. This once again demonstrates the effectiveness and robustness of RoSense in dynamic environments.

G. Sensing Range of RoSense without Moving Individuals

To further explore the sensing range of RoSense, we conducted experiments considering varying distances between the target and the LoS path, without any moving individuals in the area of interest, i.e., S16 and S17. Fig. 16 and Fig. 17 display the respiration signal patterns obtained using each method when the distances between the target and the LoS path are 10 meters in the laboratory and 25 meters in the corridor. According to these two figures, RoSense is capable of obtaining signal patterns which exhibit clear patterns related to the respiratory rate in these settings. This demonstrates that RoSense is capable of supporting room-scale remote healthcare applications.

H. Performance Comparison with Baseline Methods Designed for Dynamic Interference

To further validate the robustness of RoSense under dynamic interference, we compared it with ExRadio [51] and RespiRadio [59] in S18, S19, S20 and S21. Unlike HRD, FarSense and CSI ratio, which are primarily suitable for static scenarios, ExRadio and RespiRadio are designed to mitigate motion-induced disturbances. We conducted the comparison in the laboratory and corridor with one or two interfering individuals walking around the target. The MAE is listed in Table IV and Table V. We can see that RoSense still achieves lower MAE than ExRadio and RespiRadio across all scenarios, confirming its ability to suppress motion-induced interference. The superior performance of RoSense can be attributed to its

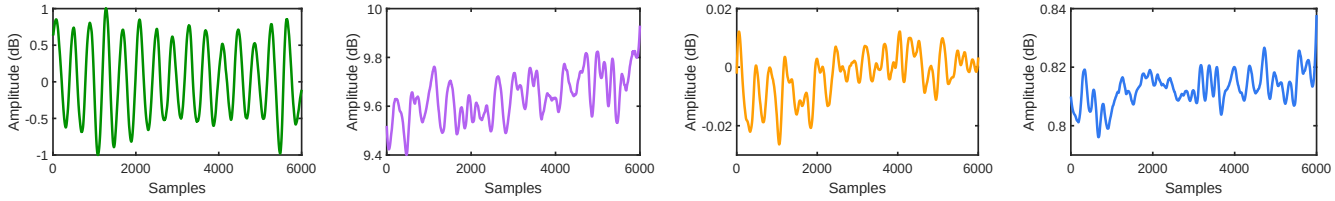

(a) RoSense, 10 meters. (b) HRD, 10 meters. (c) FarSense, 10 meters. (d) CSI ratio, 10 meters.

Fig. 16. Respiration signal patterns obtained using each method without any moving individuals in the laboratory, i.e., S16.

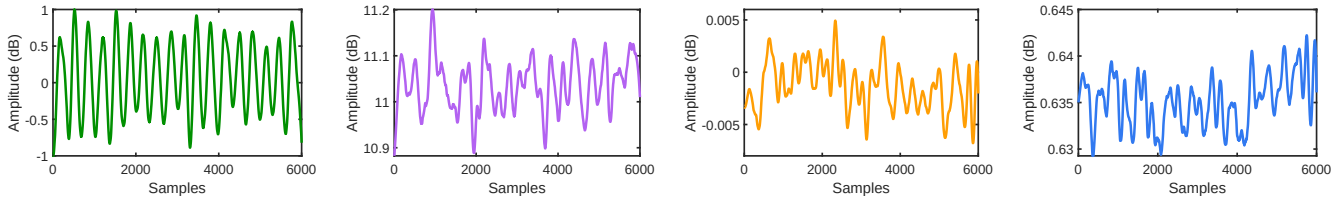

(a) RoSense, 25 meters. (b) HRD, 25 meters. (c) FarSense, 25 meters. (d) CSI ratio, 25 meters.

Fig. 17. Respiration signal patterns obtained using each method without any moving individuals in the corridor, i.e., S17.

TABLE IV
MAE OF ROSENSE AND BASELINE METHODS DESIGNED FOR DYNAMIC INTERFERENCE IN PRESENCE OF DIFFERENT NUMBER OF MOVING INDIVIDUALS IN LABORATORY

Scenarios	RoSenses	ExRadio	RespiRadio
S18	0.69	0.86	1.93
S19	0.73	0.95	1.62

TABLE V
MAE OF ROSENSE AND BASELINE METHODS DESIGNED FOR DYNAMIC INTERFERENCE IN PRESENCE OF DIFFERENT NUMBER OF MOVING INDIVIDUALS IN CORRIDOR

Scenarios	RoSenses	ExRadio	RespiRadio
S20	0.78	0.99	1.66
S21	0.81	0.92	1.89

PSD-based subcarrier selection and complementary alignment-fusion mechanism, which not only filters out corrupted subcarriers but also exploits their residual complementarity.

V. DISCUSSION

In this section, the limitations of RoSense and potential enhancements are presented.

RoSense is designed for respiration monitoring of a single subject in the presence of interfering individuals. However, in real-world scenarios, it is common to have multiple subjects and interfering individuals within the area of interest. For such sensing tasks, it is challenging to separate the signal variations induced by subjects with only commodity devices. One potential solution is to treat the multiple subjects' respiration monitoring as a blind source separation problem, which allows for the extraction of each subject's respiratory information by solving the blind source separation problem [60], [61]. Furthermore, it is essential to address the challenges of suppressing much more complex interference and noise from multiple subjects and moving individuals. Another solution is to use a larger bandwidth or an antenna array to increase the sensing resolution, enabling to separate each subject's respiratory information [62]–[64]. Additionally, a distributed antenna system or cell-free multi-input multi-output (MIMO) could be explored as an alternative. By exploiting spatially separated antennas, these systems can mitigate interference and improve sensing accuracy, making it easier to isolate individual respiration signals even in complex environments.

In our experiments, we have demonstrated the robustness and generalization of RoSense in the presence of multiple moving individuals in the laboratory and corridor settings. Moving forward, we plan to explore the sensing ability of RoSense in more complex scenarios [65]. For instance, we will deploy RoSense in real home settings that feature more cluttered conditions and a higher number of interfering individuals. Additionally, as shown in the previous experiments, RoSense is capable of maintaining satisfactory performance when the distances between the target and the LoS are 10 meters in the laboratory and 25 meters in the corridor. We will also explore the deployment of RoSense in larger indoor environments to assess the limits of its sensing range in the absence of interfering individuals.

VI. CONCLUSION

In this study, RoSense was designed and implemented on commodity Wi-Fi devices to enable robust respiration monitoring in the presence of moving individuals. The functional modules developed for RoSense allow it to fully leverage the information carried by available subcarriers and compensate for their weak periodicity parts, thereby enhancing both sensing ability and sensing range. Extensive experiments involving 10 volunteers across various practical scenarios demonstrate the feasibility and effectiveness of RoSense. Compared to baseline methods, RoSense improves deployment efficiency and supports broader applicability across diverse scenarios. The proposed RoSense is an initial attempt toward achieving

robust contactless vital sign sensing under ambient dynamics. In comparison to traditional techniques, RoSense incorporates a signal power-guided subcarrier selection strategy, offering a robust and adaptable strategy for identifying CSI components in respiration monitoring. This innovation enables RoSense to maintain strong performance in the presence of multiple moving individuals and varying LoS conditions. We envision that the developed wireless signal processing modules can serve as general methodologies applicable to other use cases.

REFERENCES

[1] Y. Yin, X. Yang, J. Xiong, S. I. Lee, P. Chen, and Q. Niu, "Ubiquitous smartphone-based respiration sensing with Wi-Fi signal," *IEEE Internet Things J.*, vol. 9, no. 2, pp. 1479–1490, 2022.

[2] Y. Zhang, Q. Ge, Z. Wang, Y. Qin, Y. Wu, M. Wang, M. Shi, L. Xue, W. Guo, Y. Zhang *et al.*, "Extracorporeal closed-loop respiratory regulation for patients with respiratory difficulty using a soft bionic robot," *IEEE Trans. Biomed. Eng.*, vol. 71, no. 10, pp. 2923–2935, 2024.

[3] L. Liu, J. Zhang, Y. Qu, S. Zhang, and W. Xiao, "mmRH: Noncontact vital sign detection with an FMCW mm-wave radar," *IEEE Sensors J.*, vol. 23, no. 8, pp. 8856–8866, 2023.

[4] R. Alam, D. B. Peden, and J. C. Lach, "Wearable respiration monitoring: Interpretable inference with context and sensor biomarkers," *IEEE J. Biomed. Health Inform.*, vol. 25, no. 6, pp. 1938–1948, 2021.

[5] J. Fan, C. Pan, G. Zhao, X. Tong, K. Li, and S. Huang, "RespEnh: A technique for enhancing respiration sensing in interference scenarios with Wi-Fi signal," *IEEE Internet Things J.*, vol. 11, no. 22, pp. 36 534–36 548, 2024.

[6] B. Huang, S. Hu, Z. Liu, C.-L. Lin, J. Su, C. Zhao, L. Wang, and W. Wang, "Challenges and prospects of visual contactless physiological monitoring in clinical study," *NPJ Digit. Med.*, vol. 6, no. 1, p. 231, 2023.

[7] I. Costanzo, D. Sen, L. Rhein, and U. Guler, "Respiratory monitoring: Current state of the art and future roads," *IEEE Rev. Biomed. Eng.*, vol. 15, pp. 103–121, 2022.

[8] L. Zheng, S. Bi, S. Wang, Z. Quan, X. Li, X. Lin, and H. Wang, "ResMon: Domain-adaptive wireless respiration state monitoring via few-shot Bayesian deep learning," *IEEE Internet Things J.*, vol. 10, no. 23, pp. 20 914–20 927, 2023.

[9] L. Gui, S. Zheng, Z. Guo, Z. Li, M. Gao, S. Dustdar, and F. Xiao, "RaliSense: Extending WiFi respiratory detection range by rapid alignment of dynamic components," *IEEE Trans. Mob. Comput.*, vol. 24, no. 9, pp. 8119–8135, 2025.

[10] W. Song, Z. Wang, Y. Guo, Z. Sun, Z. Ren, C. Chen, B. Guo, Z. Yu, X. Zhou, and D. Zhang, "FinerSense: A fine-grained respiration sensing system based on precise separation of Wi-Fi signals," *IEEE Trans. Mob. Comput.*, vol. 24, no. 5, pp. 3703–3718, 2025.

[11] Q. Gao, J. Tong, J. Wang, Z. Ran, and M. Pan, "Device-free multi-person respiration monitoring using WiFi," *IEEE Trans. Veh. Technol.*, vol. 69, no. 11, pp. 14 083–14 087, 2020.

[12] Z. Guo, W. Yuan, L. Gui, B. Sheng, and F. Xiao, "BreatheBand: A fine-grained and robust respiration monitor system using WiFi signals," *ACM Trans. Sens. Netw.*, vol. 19, no. 4, pp. 1–18, 2023.

[13] M. Chu, T. Nguyen, V. Pandey, Y. Zhou, H. N. Pham, R. Bar-Yoseph, S. Radom-Aizik, R. Jain, D. M. Cooper, and M. Khine, "Respiration rate and volume measurements using wearable strain sensors," *NPJ Digit. Med.*, vol. 2, no. 1, p. 8, 2019.

[14] Z. Li, T. Jin, X. Hu, Y. Song, J. Zhang, and Z. Sang, "Remote respiratory and cardiac motion patterns separation with 4D imaging radars," *IEEE J. Biomed. Health Inform.*, vol. 27, no. 6, pp. 1938–1948, 2023.

[15] P. Sharma, X. Hui, J. Zhou, T. B. Conroy, and E. C. Kan, "Wearable radio-frequency sensing of respiratory rate, respiratory volume, and heart rate," *NPJ Digit. Med.*, vol. 3, no. 1, p. 98, 2020.

[16] W. Xie, L. Gan, L. Huang, C. Shi, B. Liu, C.-H. Wu, Y.-T. Lee, J. Chen, and R. Zhang, "A real-time respiration monitoring system using WiFi sensing based on the concentric circle model," *IEEE Trans. Biomed. Circuits Syst.*, vol. 17, no. 2, pp. 157–168, 2023.

[17] F. Adib, H. Mao, Z. Kabelac, D. Katabi, and R. C. Miller, "Smart homes that monitor breathing and heart rate," in *Proc. 33rd Annu. ACM Conf. Hum. Factors Comput. Syst.*, 2015, pp. 837–846.

[18] Y. Yang, H. Wang, R. Jiang, X. Guo, J. Cheng, and Y. Chen, "A review of IoT-enabled mobile healthcare: Technologies, challenges, and future trends," *IEEE Internet Things J.*, vol. 9, no. 12, pp. 9478–9502, 2022.

[19] X. Shen, H. Jiang, D. Liu, K. Yang, F. Deng, T. Zhang, Z. Xiao, J. C. Lui, J. Liu, S. Dustdar *et al.*, "PupilHeart: Heart rate variability monitoring via pupillary fluctuations on mobile devices," *IEEE Internet Things J.*, vol. 10, no. 20, pp. 18 042–18 053, 2023.

[20] B. Li, Y. Ren, Y. Wang, and J. Yang, "SpaceBeat: Identity-aware multi-person vital signs monitoring using commodity WiFi," *Proc. ACM Interact. Mob. Wearable Ubiquitous Technol.*, vol. 8, no. 3, pp. 1–23, 2024.

[21] J. Zhang, Y. Li, and W. Xiao, "Integrated multiple kernel learning for device-free localization in cluttered environments using spatiotemporal information," *IEEE Internet Things J.*, vol. 8, no. 6, pp. 4749–4761, 2021.

[22] S. Dong, L. Wen, Y. Li, J. Lu, Z. Zhang, C. Yuan, and C. Gu, "Remote respiratory variables tracking with biomedical radar-based IoT system during sleep," *IEEE Internet Things J.*, vol. 11, no. 11, pp. 19 937–19 948, 2024.

[23] S. Ahmed and S. H. Cho, "Machine learning for healthcare radars: Recent progresses in human vital sign measurement and activity recognition," *IEEE Commun. Surv. Tutor.*, vol. 26, no. 1, pp. 461–495, 2024.

[24] J. Zhang, R. Xi, Y. He, Y. Sun, X. Guo, W. Wang, X. Na, Y. Liu, Z. Shi, and T. Gu, "A survey of mmwave-based human sensing: Technology, platforms and applications," *IEEE Commun. Surv. Tutor.*, vol. 25, no. 4, pp. 2052–2087, 2023.

[25] P. Kontou, S. B. Smida, and D. E. Anagnostou, "Contactless respiration monitoring using Wi-Fi and artificial neural network detection method," *IEEE J. Biomed. Health Inform.*, vol. 28, no. 3, pp. 1297–1308, 2024.

[26] W. Meng, Z. Liu, B. Li, W. Cui, J. T. Zhou, and L. Zhang, "GrapHAR: A lightweight human activity recognition model by exploring the sub-carrier correlations," *IEEE Trans. Wireless Commun.*, vol. 23, no. 4, pp. 2755–2770, 2024.

[27] J. Xiao, H. Li, M. Wu, H. Jin, M. J. Deen, and J. Cao, "A survey on wireless device-free human sensing: Application scenarios, current solutions, and open issues," *ACM Comput. Surv.*, vol. 55, no. 5, pp. 1–35, 2022.

[28] S. Tan, Y. Ren, J. Yang, and Y. Chen, "Commodity WiFi sensing in ten years: Status, challenges, and opportunities," *IEEE Internet Things J.*, vol. 9, no. 18, pp. 17 832–17 843, 2022.

[29] X. Wang, C. Yang, and S. Mao, "TensorBeat: Tensor decomposition for monitoring multiperson breathing beats with commodity WiFi," *ACM Trans. Intell. Syst. Technol.*, vol. 9, no. 1, pp. 1–27, 2017.

[30] J. Zhang, J. Xue, Y. Li, and S. L. Cotton, "Leveraging online learning for domain-adaptation in Wi-Fi-based device-free localization," *IEEE Trans. Mob. Comput.*, vol. 24, no. 8, pp. 7773–7787, 2025.

[31] B. Tan, Q. Chen, K. Chetty, K. Woodbridge, W. Li, and R. Piechocki, "Exploiting WiFi channel state information for residential healthcare informatics," *IEEE Commun. Mag.*, vol. 56, no. 5, pp. 130–137, 2018.

[32] Y. Ge, A. Taha, S. A. Shah, K. Dashtipour, S. Zhu, J. Cooper, Q. H. Abbasi, and M. A. Imran, "Contactless WiFi sensing and monitoring for future healthcare-Emerging trends, challenges, and opportunities," *IEEE Rev. Biomed. Eng.*, vol. 16, pp. 171–191, 2023.

[33] J. Zhang, Y. Li, Q. Li, and W. Xiao, "Variance-constrained local-global modeling for device-free localization under uncertainties," *IEEE Trans. Ind. Inform.*, vol. 20, no. 4, pp. 5229–5240, 2024.

[34] D. Halperin, W. Hu, A. Sheth, and D. Wetherall, "Tool release: Gathering 802.11 n traces with channel state information," *ACM SIGCOMM Comput. Commun. Rev.*, vol. 41, no. 1, p. 53, 2011.

[35] J. Zhang, Y. Li, and W. Xiao, "Toward robust and accurate device-free localization in cluttered environments with commodity WiFi devices," *IEEE Internet Things J.*, vol. 9, no. 24, pp. 24 587–24 599, 2022.

[36] V. V. Ratnam, H. Chen, H. H. Chang, A. Sehgal, and J. Zhang, "Optimal preprocessing of WiFi CSI for sensing applications," *IEEE Trans. Wireless Commun.*, vol. 23, no. 4, pp. 10 820–10 833, 2024.

[37] J. W. Browning, S. L. Cotton, P. C. Sofotasios, D. Morales-Jimenez, and M. D. Yacoub, "A Unification of LoS, Non-LoS, and Quasi-LoS signal propagation in wireless channels," *IEEE Trans. Antennas Propag.*, vol. 71, no. 3, pp. 2682–2696, 2023.

[38] S. M. Hernandez and E. Bulut, "WiFi sensing on the edge: Signal processing techniques and challenges for real-world systems," *IEEE Commun. Surv. Tutor.*, vol. 25, no. 1, pp. 46–76, 2023.

[39] Z. Wang, B. Guo, Z. Yu, and X. Zhou, "Wi-Fi CSI-based behavior recognition: From signals and actions to activities," *IEEE Commun. Mag.*, vol. 56, no. 5, pp. 109–115, 2018.

[40] L. Wang, X. Yang, S. Zhou, Z. Lu, Y. Yang, and C. Tian, "MUID: Multi-person gait identification with commodity Wi-Fi," *IEEE Trans. Instrum. Meas.*, vol. 74, no. 2, p. 9507516, 2025.

[41] J. Zhang, Y. Li, W. Xiao, and Z. Zhang, "Online spatiotemporal modeling for robust and lightweight device-free localization in nonstationary

environments," *IEEE Trans. Ind. Inform.*, vol. 19, no. 7, pp. 8528–8538, 2023.
[42] Y. Zou, W. Liu, K. Wu, and L. M. Ni, "Wi-Fi radar: Recognizing human behavior with commodity Wi-Fi," *IEEE Commun. Mag.*, vol. 55, no. 10, pp. 105–111, 2017.
[43] M. G. Moghaddam, A. A. N. Shirehjini, and S. Shirmohammadi, "A WiFi-based method for recognizing fine-grained multiple-subject human activities," *IEEE Trans. Instrum. Meas.*, vol. 72, no. 6, p. 2520313, 2023.
[44] X. Liu, J. Cao, S. Tang, J. Wen, and P. Guo, "Contactless respiration monitoring via off-the-shelf WiFi devices," *IEEE Trans. Mob. Comput.*, vol. 15, no. 10, pp. 2466–2479, 2016.
[45] H. Wang, D. Zhang, J. Ma, Y. Wang, Y. Wang, D. Wu, T. Gu, and B. Xie, "Human respiration detection with commodity WiFi devices: Do user location and body orientation matter?" in *Proc. 2016 ACM Int. Joint Conf. Pervas. Ubiquitous Comput.*, 2016, pp. 25–36.
[46] Y. Zeng, D. Wu, R. Gao, T. Gu, and D. Zhang, "FullBreathe: Full human respiration detection exploiting complementarity of CSI phase and amplitude of WiFi signals," *Proc. ACM Interact. Mob. Wearable Ubiquitous Technol.*, vol. 2, no. 3, pp. 1–19, 2018.
[47] Y. Zeng, D. Wu, J. Xiong, E. Yi, R. Gao, and D. Zhang, "FarSense: Pushing the range limit of WiFi-based respiration sensing with CSI ratio of two antennas," *Proc. ACM Interact. Mob. Wearable Ubiquitous Technol.*, vol. 3, no. 3, pp. 1–26, 2019.
[48] X. Wang, C. Yang, and S. Mao, "On CSI-based vital sign monitoring using commodity WiFi," *ACM Trans. Comput. Healthc.*, vol. 1, no. 3, pp. 1–27, 2020.
[49] B. Yu, Y. Hou, Z. Pang, and H. Zhang, "Contactless sensing-aided respiration signal acquisition using improved empirical wavelet transform for rhythm detection," *IEEE J. Biomed. Health Inform.*, vol. 27, no. 7, pp. 3141–3151, 2023.
[50] N. Zheng, Y. Li, S. Jiang, Y. Li, R. Yao, C. Dong, T. Chen, Y. Yang, Z. Yin, and Y. Liu, "AdaWiFi, collaborative WiFi sensing for cross-environment adaptation," *IEEE Trans. Mob. Comput.*, vol. 24, no. 2, pp. 845–858, 2024.
[51] J. Qiu, P. Zheng, K. Chi, R. Xu, and J. Liu, "Respiration monitoring in high-dynamic environments via combining multiple WiFi channels based on wire direct connection between RX/TX," *IEEE Internet Things J.*, vol. 10, no. 2, pp. 1558–1573, 2023.
[52] X. Xie, D. Zhang, Y. Li, Y. Hu, Q. Sun, and Y. Chen, "Robust WiFi respiration sensing in the presence of interfering individual," *IEEE Trans. Mob. Comput.*, vol. 23, no. 8, pp. 8447–8462, 2024.
[53] Y. Li, D. Wu, J. Zhang, X. Xu, Y. Xie, T. Gu, and D. Zhang, "DiverSense: Maximizing Wi-Fi sensing range leveraging signal diversity," *Proc. ACM Interact. Mob. Wearable Ubiquitous Technol.*, vol. 6, no. 2, pp. 1–28, 2022.
[54] D. Zhang, X. Li, and Y. Chen, "Pushing the limit of phase offset for contactless sensing using commodity WiFi," in *Proc. IEEE Int. Conf. Acoust. Speech Signal Process.*, 2021, pp. 8303–8307.
[55] J. Zhang, Y. Li, H. Xiong, D. Dou, C. Miao, and D. Zhang, "HandGest: Hierarchical sensing for robust in-the-air handwriting recognition with commodity WiFi devices," *IEEE Internet Things J.*, vol. 9, no. 19, pp. 19 529–19 544, 2022.
[56] R. Gao, M. Zhang, J. Zhang, Y. Li, E. Yi, D. Wu, L. Wang, and D. Zhang, "Towards position-independent sensing for gesture recognition with Wi-Fi," *Proc. ACM Interact. Mob. Wearable Ubiquitous Technol.*, vol. 5, no. 2, pp. 1–28, 2021.
[57] R. K. Pearson, Y. Neuvo, J. Astola, and M. Gabbouj, "Generalized Hampel filters," *EURASIP J. Adv. Signal Process.*, vol. 2016, pp. 1–18, 2016.
[58] Y. Zeng, D. Wu, J. Xiong, and D. Zhang, "Boosting WiFi sensing performance via CSI ratio," *IEEE Pervas. Comput.*, vol. 20, no. 1, pp. 62–70, 2021.
[59] S. Shi, Y. Xie, M. Li, A. X. Liu, and J. Zhao, "Synthesizing wider WiFi bandwidth for respiration rate monitoring in dynamic environments," in *Proc. IEEE Conf. Comput. Commun.*, 2019, pp. 181–189.
[60] Y. Zeng, D. Wu, J. Xiong, J. Liu, Z. Liu, and D. Zhang, "MultiSense: Enabling multi-person respiration sensing with commodity WiFi," *Proc. ACM Interact. Mob. Wearable Ubiquitous Technol.*, vol. 4, no. 3, pp. 1–29, 2020.
[61] J. Hu, T. Zheng, Z. Chen, H. Wang, and J. Luo, "MUSE-Fi: Contactless multi-person sensing exploiting near-field Wi-Fi channel variation," in *Proc. 29th Annual Int. Conf. Mob. Comput. Network.*, 2023, pp. 1–15.
[62] L. Guan, Z. Zhang, X. Yang, N. Zhao, D. Fan, M. A. Imran, and Q. H. Abbasi, "Multi-person breathing detection with switching antenna array based on WiFi signal," *IEEE J. Transl. Eng. Health Med.*, vol. 11, pp. 23–31, 2023.
[63] R. Du, H. Hua, H. Xie, X. Song, Z. Lyu, M. Hu, Y. Xin, S. McCann, M. Montemurro, T. X. Han *et al.*, "An overview on IEEE 802.11bf: WLAN sensing," *IEEE Commun. Surv. Tutor.*, vol. 27, no. 1, pp. 184–217, 2024.
[64] J. A. Zhang, M. L. Rahman, K. Wu, X. Huang, Y. J. Guo, S. Chen, and J. Yuan, "Enabling joint communication and radar sensing in mobile networks-A survey," *IEEE Commun. Surv. Tutor.*, vol. 24, no. 1, pp. 306–345, 2022.
[65] H. Zhang, Z. Wang, Z. Sun, W. Song, Z. Ren, Z. Yu, and B. Guo, "Understanding the mechanism of through-wall wireless sensing: A model-based perspective," *Proc. ACM Interact. Mob. Wearable Ubiquitous Technol.*, vol. 6, no. 4, pp. 1–28, 2023.

APPENDIX

To justify our empirical observation that a subset of subcarriers remains resilient under dynamic interference, we analyze the underlying signal model in the Appendix.

The CSI at frequency f and time t can be represented as

$$H(f,t) = \sum_{p} A_p(f,t)\, e^{-j2\pi \frac{d_p(t)}{\lambda}} + \epsilon(t) \tag{A.1}$$

where $A_p(f,t)$ is the complex attenuation of the p-th path, $d_p(t)$ is the propagation length, λ is the wavelength of the signal, and $\epsilon(t)$ is the random noise, often modeled as additive white Gaussian noise.

Respiratory motion introduces small and periodic variations in the chest displacement, resulting in subtle changes in the propagation paths. The received CSI can be decomposed into static and dynamic components. The dynamic component corresponds to the paths reflected from the target while the static component consists of the LoS propagation and other paths from static objects in the environment. Therefore, the CSI can be reformulated as

$$H(f,t) = A(f,t)\, e^{-j2\pi \frac{d(t)}{\lambda}} + H_s(f,t) + \epsilon(t) \tag{A.2}$$

where $H_s(f,t)$ is the static component, $A(f,t)$, $e^{-j2\pi \frac{d(t)}{\lambda}}$ and $d(t)$ are the complex attenuation, phase shift and path length of the dynamic component, respectively.

In real-world scenarios, the presence of a walking interfering individual in front of the target causes the received signal to be influenced by both the target-induced reflections and the interferer-induced perturbations. Mathematically, Eq. (A.2) can be rewritten into the composite model:

$$\begin{aligned} H(f,t) = {} & A(f,t)\, e^{-j2\pi \frac{d(t)}{\lambda}} + H_s(f,t) \\ & + A_m(f,t)\, e^{-j2\pi \frac{d_m(t)}{\lambda}} + \epsilon(t) \end{aligned} \tag{A.3}$$

where $A_m(f,t)\, e^{-j2\pi \frac{d_m(t)}{\lambda}}$ is the interference component generated by the moving individual.

In this case, a moving individual introduces variations in path delay, and the exponential term amplifies these variations differently across subcarriers. As a result, this frequency-dependent amplification causes the interference to be strong on certain subcarriers while relatively weak on others [52]. Additionally, a moving individual alters only a few multipath components at any moment. Since each path produces a different frequency response, the interference contaminates only a subset of subcarriers instead of all subcarriers uniformly. Leveraging this characteristic, PSD-based subcarrier selection identifies the subcarriers with less interference by evaluating the spectral stability in the respiration frequency range.

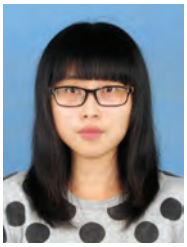

Yanjiao Li (Member, IEEE) received the Ph.D. degree from the University of Science and Technology Beijing, Beijing, China, in 2019.

She is currently an Assistant Professor with the Institute of Engineering Technology, University of Science and Technology Beijing, and also a Marie Curie Research Fellow with the School of Electronic and Electrical Engineering, University of Leeds, U.K. From 2019 to 2021, she was a Postdoctoral Research Fellow with the Beijing Institute of Technology, China. She was a Visiting Research Fellow with the University of Leeds in 2018. Her current research interests include modeling and optimization for complex systems, and machine learning.

Dr. Li was a recipient of the Marie Sklodowska-Curie Actions Postdoctoral Fellowships (MSCA-PF), European Commission.

Jie Zhang (Senior Member, IEEE) is currently a Lecturer (Assistant Professor) with the Centre for Wireless Innovation, Queen's University Belfast, U.K. From 2022 to 2024, he was a Marie Curie Research Fellow with the University of Leeds, U.K. He was an Associate Professor with the University of Science and Technology Beijing, China, in 2022. From 2019 to 2021, he was a Postdoctoral Research Fellow with the Peking University, China. He was a Visiting Research Fellow with the University of Leeds in 2018. His current research interests include intelligent sensing, wireless systems, AIoT, wearable computing, and machine learning.

Dr. Zhang serves as an Associate Editor for IEEE Transactions on Neural Networks and Learning Systems. He was a recipient of the Marie Sklodowska-Curie Actions Individual Fellowships (MSCA-IF), European Commission.

Qing Li received the Ph.D. degree from the University of Science and Technology Beijing, Beijing, China, in 2000.

He is currently a Full Professor with the School of Automation and Electrical Engineering, University of Science and Technology Beijing. From 2006 to 2007, he was a Visiting Scholar with the Ryerson University, Toronto, Canada. His research interests include intelligent control, intelligent optimization, machine learning and IoT.

Yang Li received the Ph.D. degree from the Peking University, Beijing, China, in 2025. He is currently with the Huawei Technologies Company Ltd., China. His research interests include wireless sensing and mobile computing.

Hien Quoc Ngo (Fellow, IEEE) is currently a Professor with the Centre for Wireless Innovation, Queen's University Belfast, U.K. He is also an Eminent Scholar at Kyung Hee University, South Korea. His main research interests include cellular/cell-free massive MIMO systems, integrated sensing and communications, reconfigurable intelligent surfaces, and physical layer security. He has authored and co-authored many research papers in wireless communications, and co-authored the Cambridge University Press textbook "Fundamentals of Massive MIMO" (2016).

Dr. Ngo received the IEEE ComSoc Stephen O. Rice Prize in 2015, the IEEE ComSoc Leonard G. Abraham Prize in 2017, the Best Ph.D. Award from EURASIP in 2018, and the IEEE CTTC Early Achievement Award in 2023. He also received the IEEE Sweden VT-COM-IT Joint Chapter Best Student Journal Paper Award in 2015. He was awarded the UKRI Future Leaders Fellowship in 2019. He serves as the Editor for IEEE Transactions on Wireless Communications, IEEE Transactions on Communications, Digital Signal Processing, and Physical Communication (Elsevier). He was an Editor of the IEEE Wireless Communications Letters, a Guest Editor of IET Communications, and a Guest Editor of IEEE ACCESS in 2017.

Trung Q. Duong (Fellow, IEEE) is a Canada Excellence Research Chair (CERC) and a Full Professor at Memorial University, Canada. He is an Adjunct Professor at Queen's University Belfast, U.K. He is also a Visiting Professor at Kyung Hee University, South Korea, at Edinburgh Napier University, U.K., and at Duy Tan University, Vietnam. His current research interests include wireless communications, quantum machine learning, and quantum optimization.

Dr. Duong is the Editor-in-Chief of IEEE Communications Surveys & Tutorials and an IEEE ComSoc Distinguished Lecturer. He has received two prestigious awards from the U.K. Royal Academy of Engineering (RAEng): the RAEng Research Chair and the RAEng Research Fellow. He was a recipient of the prestigious Newton Prize 2017. He is a Fellow of the Engineering Institute of Canada (EIC), the Canadian Academy of Engineering (CAE), the Institution of Engineering and Technology (IET), and Asia-Pacific Artificial Intelligence Association (AAIA).

Simon L. Cotton (Fellow, IEEE) is currently a Full Professor and the Director of the Centre for Wireless Innovation, Queen's University Belfast, U.K. He was a Reader (Associate Professor) and a Lecturer (Assistant Professor) (2012-2019), also a Senior Research Fellow (2011-2012), and a Research Fellow (2007-2011) with Queen's University Belfast. He has authored and co-authored over 220 publications in major IEEE/IET journals and refereed international conferences, three book chapters, and three patents. His current research interests include radio channel measurements, characterisation and modelling, body-centric communications, and mobile-to-mobile communications.

Dr. Cotton was a recipient of the H. A. Wheeler Prize, IEEE Antennas and Propagation Society, and the Sir George Macfarlane Award, U.K. Royal Academy of Engineering.